frontiers in Materials

ORIGINAL RESEARCH
published: 03 August 2018
doi: 10.3389/fmats.2018.00031

Catalyst Screening for Oxidative Coupling of Methane Integrated in Membrane Reactors

*Julio Garcia-Fayos, Maria P. Lobera, Maria Balaguer and Jose M. Serra**

Instituto de Tecnología Química, Universitat Politècnica de València, Consejo Superior de Investigaciones Científicas, Valencia, Spain

Increased availability of methane from shale gas and stranded gas deposits in the recent years may facilitate the production of ethylene by means of potentially more competitive routes than the state-of-the-art steam cracking processes. One appealing route is the oxidative coupling of methane (OCM), which is considered in this work for the production of ethylene by means of the use of catalytic membrane reactors (CMR) based on $Ba_{0.5}Sr_{0.5}Co_{0.8}Fe_{0.2}O_{3-\delta}$ (BSCF) ceramic material. In a first approach, a screening of 15 formulations as catalysts for the ethylene-ethane production was conducted on CMR consisting of disk-shaped planar BSCF membranes. At 900°C, the maximum C_2 selectivity was 70%, reached with $Ba_{0.5}Sr_{0.5}FeO_{3-\delta}$ and $La_{0.5}Ce_{0.1}Sr_{0.4}Co_{0.8}Fe_{0.2}O_{3-\delta}$ catalysts. On the other hand, low CH_4 conversions (X_{CH4}) resulted in C_2 yields below 3%. Operation at 1,000°C significantly shifted X_{CH4} for all the activated membranes due to the decrease in CH_4/O_2 ratios, thus obtaining C_2 yields close to 9% and productivities of ca. 1.2 ml·min^{-1}·cm^{-2} with $Ce_{0.9}Gd_{0.1}O_{2-\delta}$ and $Ba_{0.5}Sr_{0.5}Co_{0.8}Fe_{0.2}O_{3-\delta}$ impregnated with Mn-Na_2WO_4 catalysts. The performance of OCM reaction was also studied in a tubular catalytic membrane reactor. Tubular configuration improved C_2 yield by minimizing CH_4/O_2 ratios up to 1.7, obtaining a maximum of 15.6% at 900°C with a BSCF capillary membrane activated with a packed bed of 2 wt% Mn/5 wt% Na_2WO_4 on SiO_2 catalyst.

Keywords: catalytic membrane reactor, oxygen transport membrane, BSCF, OCM, ethylene production, ionic conductor

Edited by:
David Alfredo Pacheco Tanaka, Tecnalia, Spain

Reviewed by:
Jose A. Medrano, Eindhoven University of Technology, Netherlands
Tridib Kumar Sinha, Gyeongsang National University, South Korea

****Correspondence:***
Jose M. Serra
jmserra@itq.upv.es

Specialty section:
This article was submitted to Functional Ceramics, a section of the journal Frontiers in Materials

Received: *19 February 2018*
Accepted: *11 May 2018*
Published: *03 August 2018*

Citation:
Garcia-Fayos J, Lobera MP, Balaguer M and Serra JM (2018) Catalyst Screening for Oxidative Coupling of Methane Integrated in Membrane Reactors. Front. Mater. 5:31. doi: 10.3389/fmats.2018.00031

INTRODUCTION

Ethylene is the most demanded organic compound worldwide, with a yearly production of 150 Mton in 2016 (Reporters, 2016). It is probably the most important basic petrochemical since it is used for producing other essential chemicals in nowadays economy, such as polyethylene, ethylene oxide, acetaldehyde or alcohols. Currently, ethylene is mainly produced by steam cracking of hydrocarbon feedstocks (naphta, gasoil, and condensates). Amongst all the existing feedstocks, ethane cracking is the most preferred, since almost no coproducts are obtained. Steam cracking is a non-catalytic process run at very high temperatures (typically 850°C). The main drawbacks are the process complexity and the downstream processing, the high energy requirements due to the endothermic reaction, and the operation complications due to the high coke formation rate. Despite the high maturity of the technology no major advances are foreseen for overcoming these weaknesses.

Step 1: $CH_4 + 2O_2 \rightarrow CO_2 + 2H_2O$
Step 2: $2CH_4 + 0.5O_2 \rightarrow C_2H_6 + H_2O$
Step 3: $CH_4 + O_2 \rightarrow CO + H_2O + H_2$
Step 4: $CO + 0.5O_2 \rightarrow CO_2$
Step 5: $C_2H_6 + 0.5O_2 \rightarrow C_2H_4 + H_2O$
Step 6: $C_2H_4 + 2O_2 \rightarrow 2CO + 2H_2O$
Step 7: $C_2H_6 \rightarrow C_2H_4 + H_2$
Step 8: $C_2H_4 + 2H_2O \rightarrow 2CO + 4H_2$
Step 9: $CO + H_2O \rightarrow CO_2 + H_2$
Step 10: $CO_2 + H_2 \rightarrow CO + H_2O$

FIGURE 1 | Simplified OCM reaction mechanism presented by Stansch et al. (1997).

In the past recent years, ethylene production is focused on the use of light alkanes such as propane, ethane, and methane, mainly due to the more economic availability from shale gas and stranded gas exploitations that facilitate cost-competitive routes for the production of light olefins. Therefore, by considering these available feedstocks, several routes are being studied and developed for the production of ethylene from ethane such as the oxidative de-hydrogenation of ethane (ODHE) (Bhasin et al., 2001; Grubert et al., 2003), and from methane such as methanol-to-olefins reaction (Keil, 1999; Chen et al., 2005), Fischer-Tropsch synthesis (Lunsford, 2000), and the Oxidative Coupling of Methane (OCM) (Keller and Bhasin, 1982; Ito and Lunsford, 1985; Amenomiya et al., 1990; Lunsford, 1995). Amongst these, the use of CH_4 for the production of valuable chemicals is preferred due to economic reasons (Mleczko and Baerns, 1995; Mleczko et al., 1996), and in particular OCM is considered one of the most attractive options as a direct route for the direct conversion of CH_4 into C_2H_4.

The first works on OCM were reported in the early 80′s by Keller and Bhasin (1982). Since then, OCM has attracted much attention from both the academia and industry. A big number of developments were mainly focused on catalysts that maximize C_2H_4 yields and optimizing the reactor design for managing heat and streams (Otsuka et al., 1986; Hutchings et al., 1989; Amenomiya et al., 1990; Maitra, 1993; Mleczko et al., 1996). With regard to OCM reaction mechanism, Stansch et al. (1997) presented a kinetic model (**Figure 1**) where C_2H_4 formation mechanism involves a dehydrogenation step to form the radical $CH_3^{\cdot}$ species, first producing C_2H_6 by $CH_3^{\cdot}$ coupling (step 2) and then C_2H_4 by ethane dehydrogenation (steps 5 and 7). Since CH_4 is a very stable molecule, the CH_4 activation for the coupling requires breaking a strong C-H bond (ca. 439 kJ·mol^{-1}). Issues such as thermodynamic limitations for CH_4 conversion, low C_2 selectivity and catalysts deactivation due to coke formation, make OCM practically and commercially inviable (Karakaya et al., 2017). The techno-economical threshold for considering OCM as commercially available is set at 30% C_2 yield per single-pass (Farrell et al., 2016; Spallina et al., 2017).

Catalytic Membrane Reactor (CMR) technology (Aseem and Harold, 2018) with the integration of Oxygen Transport Membranes (OTMs) (Tenelshof et al., 1995; Zeng et al., 1998; Akin and Lin, 2002; Sunarso et al., 2008) is a suitable option for overcoming these drawbacks. As can be seen in the model depicted in **Figure 1**, the OCM reaction performance is affected by several secondary reactions leading to undesirable CO_x formation, mainly due to an O_2 feeding excess. Therefore, one of the main aspects of OTMs for their application in OCM reaction is the dosing of O_2 in a controlled manner by tuning parameters such as temperature, pO_2 at feed side, residence time and space velocity by reactant gas stream flow variation, etc. Therefore, by adjusting conveniently the CH_4/O_2 stoichiometry the complete oxidation of CH_4 to CO_x can be avoided, while increasing C_2 selectivity. In addition, higher conversion can be reached without safety problems related to flammability limits in conventional co-feeding reactors.

Several research groups have performed OCM reactions by considering different OTM materials, geometries and catalysts for improving the reaction toward C_2 formation. In **Table 1**, some of the reported results are summarized. Tubular geometries are preferred for conducting OCM in CMRs, with a special emphasis in the use of catalysts that improve C_2 selectivity. Amongst all the considered cases, the best results have been obtained by Othman et al. reaching a C_2 yield of 39% on a LSCF hollow fiber activated with $Bi_{1.5}Y_{0.3}Sm_{0.2}O_{3-\delta}$ catalyst.

Oxygen transport membranes consist of gastight Mixed Ionic Electronic Conductors (MIEC) that diffuse oxygen through vacancies in the crystal lattice, and simultaneously transport electrons in the opposite direction, thus obviating the need for an external electrical short circuit. Their major advantage is an infinite oxygen selectivity, assuming no leakage through the membrane layer or the sealing, and resulting in high purity oxygen that can be directly provided to oxyfuel power plants or chemical processes. Oxygen permeation through the bulk material is governed by the Wagner equation[1], favored by increasing temperatures and chemical gradients across the membrane. On the other hand, thin membranes (below 50 μm) are strongly limited by the surface exchange kinetics of molecular oxygen.

In addition to the benefits of OTMs application in the conduction of OCM reaction, the possibility of adding catalytic layers consisting of MIEC active materials may produce an increase in the rate of surface reactions (Lobera et al., 2012b). The use of catalysts based on perovskites and fluorite compounds is of great interest due to their ionic-electronic conductive properties allowing the presence of ionic oxygen species at the materials surface. Therefore, the OCM reaction can take place all over the catalytic layer at the active sites localized on the oxygen vacancies on the surface of catalyst particles. Nano-structured materials leading to highly porous catalytic layers may improve the OCM performance by ensuring a proper gas diffusion media as well as a

[1] $J(O_2) = \frac{RT}{16F^2L}\int_{pO_2'}^{pO_2''}\sigma_{amb}dlnpO_2$
where $J(O_2)$ is the oxygen permeation, R is the gas constant, T is the temperature, F is the Faraday′s constant, L is the membrane thickness, pO_2" and pO_2' stand for the O_2 partial pressures at feed and permeate sides, respectively, and σ_{amb} is the ambipolar conductivity of the membrane material.

TABLE 1 | C_2 selectivity and yield for different OCM studies conducted on CMRs.

Material	T (°C)	Geometry	Catalyst	S_{C2} (%)	Y_{C2} (%)	References
$Bi_{1.5}Y_{0.3}Sm_{0.2}O_{3-3}$	900	Tubular	–	54	35	Akin and Lin, 2002
BSCF	850	Tubular	La-Sr/CaO	66	15	Wang et al., 2005
BSCF	900	Disk	La-Sr/CaO	65	18	Olivier et al., 2009
LSCF	950	Hollow fiber	–	43.8	15.3	Tan and Li, 2006
LSCF	975	Hollow fiber	$SrTi_{0.9}Li_{0.1}O_3$	40	21	Tan et al., 2007
LSCF	900	Hollow fiber	$Bi_{1.5}Y_{0.3}Sm_{0.2}O_{3-\delta}$	79	39	Othman et al., 2015
BCFZ	800	Hollow fiber	$Mn\text{-}Na_2WO_4/SiO_2$	50	17	Czuprat et al., 2010
BCGCF	850	Tubular	Na-W-Mn	67.4	34.7	Bhatia et al., 2009

high specific surface area. Additionally, by properly doping with metal cations presenting different ionic radii, oxidation states and redox behavior, it is possible to improve the catalytic activity by increasing the number of oxygen vacancies and by varying the O-cation bond strength (Sunarso et al., 2008).

The present work is focused on the development of catalytic membrane reactors (CMR) for the production of C_2H_4 through the OCM reaction. For that aim, a screening of 15 catalyst formulations was performed on $Ba_{0.5}Sr_{0.5}Co_{0.8}Fe_{0.2}O_{3-\delta}$ (BSCF) planar membranes, following the CH_4 conversion, C_{2+} selectivity, C_{2+} yield, and C_{2+} production. The catalyst study was mainly focused on the use of different MIEC catalysts and by considering state-of-the-art OCM catalysts. Furthermore, a study on the influence of reactor geometry on OCM performance was conducted by considering a BSCF capillary activated with a $Mn\text{-}Na_2WO_4$ on SiO_2 catalytic packed bed.

EXPERIMENTAL

Dense $Ba_{0.5}Sr_{0.5}Co_{0.8}Fe_{0.2}O_{3-\delta}$ planar membranes of 15 mm diameter and 0.8 mm thickness were prepared by uniaxial pressing at 150 kN, and subsequently sintered in air for 5 h at 1,100°C. BSCF powder was provided by Fraunhofer Institute for Ceramic Technologies and Systems (IKTS, Germany). The catalysts for the activation of membranes can be grouped in (i) MIEC perovskites, (ii) lanthanide doped cerias, (iii) MgO, and (iv) LaSr/CaO. The catalysts based on MIEC perovskites consisted of $ABO_{3-\delta}$ formulations, obtained by doping *A*- and *B*-sites according to $A_{0.6}Sr_{0.4}Co_{0.5}Fe_{0.5}O_{3-\delta}$ and $Ba_{0.6}Sr_{0.4}BO_{3-\delta}$ formulations where *A* = La, Pr, Ba, Ce, Sm, and Nd and *B* = Fe and Co. MIEC catalysts powders were synthesized by Pechini method. For each catalyst, metal precursor nitrates were mixed in distilled water in order to obtain a clear solution. After complete dissolution, citric acid was added as a chelating agent, and ethylene glycol was added to polymerize with the chelating agent and produce an organometallic polymer (in a molar ratio 1:2:4 with respect to nitrates solution, citric acid, and ethylene glycol, respectively). This complexation was followed by dehydration at low temperature (up to 270°C) and finally, thermal decomposition of the precursors at 600°C formed the desired structural phases. Regarding the fluorite compounds, two different catalyst based on the system $Ce_{1-x}Ln_xO_{2-\delta}$ (x = 0.1; Ln = Tb, and Gd) were prepared by co-precipitation method. This technique consists of the dissolution of commercial lanthanide nitrates mixture in distilled water at 50°C. $(NH_4)_2CO_3$ solution in a 1:1.5 molar ratio was dropped to achieve the total precipitation of the mixed cations. The resulting precursor powder was dried at 100°C after filtration and rinsing. MgO powders were supplied by Sigma-Aldrich. LaSr/CaO catalyst was prepared by co-precipitation method being the nominal composition 10 wt% La, 20 wt% Sr on CaO.

Catalytic activation of planar membranes was conducted by screen printing catalyst porous layers on one of the sides of the membrane, which will be exposed to the reaction. The screen printing ink consists of the ceramic powder, an organic binder (ethylcellulose) and a plasticizer (terpineol), mixed and subsequently refined in a three-roll mill. The ink is printed on the membrane surface through a 9 mm diameter mesh. Finally, the coated membranes were calcined in air at T = 1,010–1,050°C for 2 h.

The OCM experimental setup is illustrated in **Figure 2**. Gold O-ring gaskets were used for membranes sealing. Synthetic air (200 ml·min^{-1}) was fed into the feed side while a dilution of 10% methane in argon (100 ml·min^{-1}) was used as the sweep gas on the reaction side.

BSCF membranes with tubular geometry were acquired from Fraunhofer IKTS. BSCF capillaries were manufactured by plastic extrusion as described in Schulz et al. (2012), obtaining tubes with a length of 220 mm, an outer diameter of 3.25 mm, and an inner diameter of 2.55 mm, resulting in a wall thickness of 0.35 mm. The capillaries were dead-ended (sealed at one tube end). The capillary capping was made by joining a flat small disk by reactive air brazing (Erskine et al., 2002). Catalytic activation of BSCF capillary was done with a packed-bed consisting of 255 mg of $Mn\text{-}Na_2WO_4/SiO_2$ catalyst (d_p = 0.4–0.6 mm) and SiC in a relation 50% v/v. The experimental set-up used for conducting the tests on BSCF capillaries is depicted in **Figure 3**. The capillary exposed area was ∼3.15 cm^2, corresponding to a capillary length of 3 cm. The contact of the rest of the capillary with the reactant gases was avoided by placing a quartz tube–acting as *liner*- above the packed-bed all along the capillary. This quartz tube presents an inner diameter of 3.75 mm, being sufficient for wrapping completely the BSCF capillary. Top and bottom inlets of the tube were blocked, thus avoiding the reactant gases to be in contact with the membrane. This was done mainly for performing the OCM tests in the 3 cm-long isothermal zone of the used furnace, thus ensuring a constant temperature in all the reaction media. Same gas stream compositions and flow rates were used as for the tests using planar membranes.

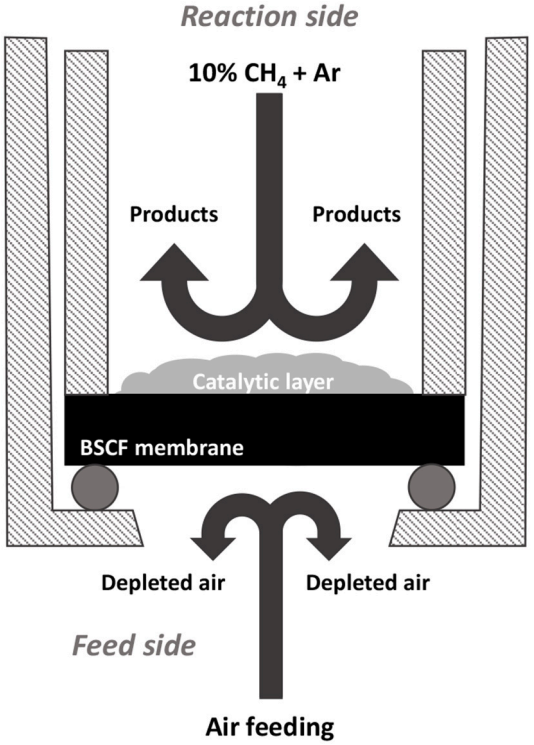

FIGURE 2 | Schematic representation of the CMR used for planar membranes tests.

Complete analysis of gases at both sides of the membrane was performed by gas chromatography (micro-GC Varian CP-4900 equipped with Molsieve5A, Pora-Plot-Q glass capillary, and CP-Sil modules). The flow and composition of the gas streams were individually controlled. Membrane gas-leak-free conditions were confirmed by continuously monitoring the N_2 concentration in the gas stream exiting the catalyst chamber. An acceptable sealing was achieved when the ratio between the oxygen flow leak and the oxygen flux was lower than 1%. The temperature was measured by a thermocouple attached to the membrane (reaction side). A proportional–integral–derivative (PID) controller maintained temperature variations within 2°C of the set point. For evaluating the reaction performance, parameters such as methane conversion (X_{CH4}), C_{2+}-hydrocarbons selectivity (S_{C2+}) and yield (Y_{C2+}), and ethylene productivity are determined from GC compounds analysis. The equations for the determination of these parameters are herein presented:

$$X_{CH4} = \frac{\sum_i n_i \cdot F_i^{out}}{F_{CH4}^{out} - \sum_i n_i \cdot F_i^{out}} \cdot 100 \quad (1)$$

$$S_{C2+} = \frac{n_{C2+} \cdot F_{C2}^{out}}{\sum_i n_i \cdot F_i^{out}} \cdot 100 \quad (2)$$

$$Y_{C2+} = 0.01 \cdot X_{CH4} \cdot S_{C2} \quad (3)$$

$$C_{2+}\ productivity = \frac{Y_{C2+} \cdot Q_{CH4}^{in}}{A_{effective}} \quad (4)$$

Where i includes all the species with carbon atoms in the products gas stream, F is the flow rate of the species expressed in mol·min^{-1}, n_i is the number of carbon atoms of component i, Q_{CH4}^{in} is the initial CH_4 flow rate (in ml·min^{-1}) and $A_{effective}$ is the effective membrane area for OCM reaction.

RESULTS AND DISCUSSION

In a first approach, the OCM reaction was studied on BSCF disk-shaped planar membranes with thicknesses of 0.8 mm. As previously observed (Lobera et al., 2011, 2012a,b, 2017), surface catalytic activation of oxygen membranes produces a performance improvement of the chemical reactions, especially ethylene production. This is mainly due to the presence of active elements towards CH_4 activation. Therefore, by considering catalyst particles with high O^{2-} mobility and redox properties, products selectivity and yield can be significantly increased. Furthermore, the presence of porous structures increases the specific surface area, enlarging the number of active sites and improving gas flow dynamics for a better gas diffusion. Then, the activation of a BSCF membrane with several known active catalysts was considered (Lobera et al., 2011, 2012a,b, 2017). On **Table 2**, all the tested membranes are listed indicating the specifications of the catalytic layers.

All the catalysts were subjected to the same conditions of temperature and pO_2, necessary to seal the membrane and be used as a CMR for OCM, so the final microstructure depends on the sintering behavior of each catalyst material under these preparation and sealing conditions. **Figure 4**, shows SEM images of some of the activated BSCF membranes. As expected, different layer morphologies are obtained depending on the deposited material, which will also play a role on the catalytic performance of each porous layer. A highly porous structure of 15 μm is obtained when depositing a BSCF layer and subsequently sintering at 1,010°C (**Figure 4b**). NdSCF, SmSCF, and LaCeSCF catalysts (**Figures 4c,e,f**) present a layer thickness in the range of 12–15 μm and also lower porosity degree than BSCF layer. LaSr/CaO activation (**Figure 4d**) layer, on the other hand, resulted in negligible porosity.

The activated BSCF membranes were tested at 900°C. Gas feed rate was 200 ml·min^{-1} of synthetic air (21% O_2) and, as sweep gas, a reactant gas stream consisting of 100 ml·min^{-1} of 10% CH_4 in argon was employed in the reaction chamber. Under these conditions, the O_2 resulting from membranes permeation was in the range of 1.16–1.68 ml·min^{-1}·cm^{-2}, corresponding therefore to CH_4/O_2 ratios of 7.5–11. The obtained results are shown in **Figure 5**, where CH_4 conversion, selectivity toward C_{2+} production, C_{2+} yield, and C_{2+} productivity are presented for each catalyst. The best results are obtained with the BSF_1010 activated membrane, reaching nearly 70% of C_{2+} selectivity, two fold the C_{2+} selectivity obtained with a non-activated BSCF membrane. Similar results were also observed in an ODHE catalytic study conducted on BSCF membranes where, despite the lower reducibility of BSF, higher C_{2+} selectivity was obtained (Lobera et al., 2012a). This can be related to a more suitable capability of BSF for conducting the $CH_3^{\cdot}$ coupling regardless

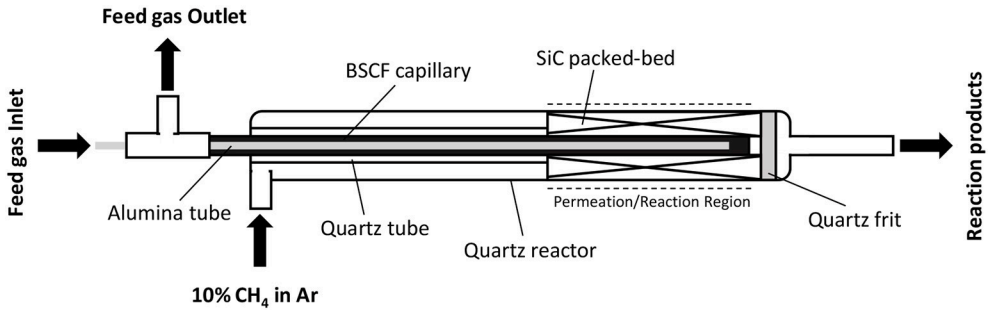

FIGURE 3 | Simplified diagram of the lab-scale reactor for the conduction of capillary membrane studies.

TABLE 2 | Catalysts for the activation of BSCF membranes.

Label	Catalyst	$T_{sintering}$ (°C)	Layer thickness (μm)
Bare	None	–	–
BSCF_1050	$Ba_{0.5}Sr_{0.5}Co_{0.8}Fe_{0.2}O_{3-\delta}$	1,050	6
BSCF_1010	$Ba_{0.5}Sr_{0.5}Co_{0.8}Fe_{0.2}O_{3-\delta}$	1,010	13
3 BSCF_1010	$Ba_{0.5}Sr_{0.5}Co_{0.8}Fe_{0.2}O_{3-\delta}$	1,010	26
3 BSCF_1010/Mn-Na_2WO_4	$Ba_{0.5}Sr_{0.5}Co_{0.8}Fe_{0.2}O_{3-\delta}$ porous layer impregnated with 2 wt% Mn/5 wt% Na_2WO_4 on SiO_2	1,010	26
NdSCF	$Nd_{0.6}Sr_{0.4}Co_{0.8}Fe_{0.2}O_{3-\delta}$	1,050	12
SmSCF	$Sm_{0.6}Sr_{0.4}Co_{0.8}Fe_{0.2}O_{3-\delta}$	1,050	14
LaSr/CaO	LaSr/CaO	1,050	12
LaCeSCF	$La_{0.5}Ce_{0.1}Sr_{0.4}Co_{0.8}Fe_{0.2}O_{3-\delta}$	1,050	13
LaPrBaSCF	$(La_{0.375}Pr_{0.375}Ba_{0.25})_{0.58}Sr_{0.4}Fe_{0.8}Co_{0.2}O_{3-\delta}$	1,050	14
BSF_1050	$Ba_{0.5}Sr_{0.5}FeO_{3-\delta}$	1,050	14
BSF_1010	$Ba_{0.5}Sr_{0.5}FeO_{3-\delta}$	1,010	12
MgO	MgO interlayer	1,050	5
MgO-Mn-Na_2WO_4	MgO interlayer impregnated with 2 wt% Mn / 5 wt% Na_2WO_4 on SiO_2	1,050	5
CeTbO	$Ce_{0.9}Tb_{0.1}O_{2-\delta}$	1,050	14
CeGdO	$Ce_{0.9}Gd_{0.1}O_{1.95}$	1,050	12

its lower redox properties leading to a lower CH_4 abstraction and subsequently, to a lower methane conversion. LaCeSCF and BaLaPrSCF activated membranes also present higher C_{2+} selectivity than BSCF (S_{C2+} in the range of 27–34%), with values of 64.7 and 58.2%, respectively. This improvement is ascribed to the incorporation of cations with mixed valence (Ce and Pr) in the A lattice position, that results in the modification in the redox behavior. The latter seems to alleviate the acidity increase resulting from the doping with cations presenting higher oxidation states (Zhou et al., 2008) that would lead to secondary reactions and to a loss in C_{2+}. This gain in catalyst basicity is observed for SmSCF, which yields better C_{2+} selectivity than BSCF, being above 55%, whereas a more basic NdSCF performs similarly to BSCF. With regard to the lanthanide-doped cerias (CeTbO and CeGdO) the better performance is attributed to the combination of high oxygen-ion mobility and their better red-ox properties (Balaguer et al., 2011). The performance of LaSr/CaO catalyst regarding S_{C2+} is lower than the observed in the literature (Wang et al., 2005; Olivier et al., 2009) due to the lower surface specific area that the catalytic layer presents in this work (**Figure 4d**), resulting in a lesser number of accessible active sites, as well as a hindrance for the gas diffusion on the catalytic media. The low selectivity (13–15%) observed for the membranes activated with MgO interlayer is expected from to the low activity of MgO in the formation of $CH_3\cdot$ radicals (Pak et al., 1998) and the observed deactivation of MgO catalysts with OCM reaction time (Wang et al., 1995; Pak et al., 1998). It is also significant the low C_{2+} selectivity observed for the membrane activated with Mn-Na_2WO_4 on SiO_2 catalyst. Only a S_{C2+} of 30% is obtained, when previous studies show C_{2+} selectivity of up to 80% (Farrell et al., 2016). The reason for such a low result can stem from the reaction between SiO_2 and BSCF leading to the formation of a SiO_2 layer on membrane surface and to the partial blocking of O_2 permeation (Thaler et al., 2016). Moreover, SiO_2 sintering and transition to α-Cristobalite from amorphous silica (catalyst support) also results in a loss of selectivity (Palermo et al., 1998; Asadi et al., 2012). It is worthy to mention that BSCF membrane activation with a BSCF porous layer does not entail a performance improvement in all the systems. Some of them present lower C_{2+} selectivity as compared with the bare membrane, which can be related with a gas diffusion hindrance resulting from the layer deposition, thus preventing CH_4 to reach the active sites or due to a fast recombination of surface O^{2-} into gaseous O_2, which would react with CH_4 causing combustion, and making these catalysts not useful for the system in a first approach. Concerning CH_4 conversion (**Figure 5A**) the obtained results are in the range of 2–8%, with MgO and MgO_Mn-Na_2WO_4 yielding the highest methane conversion rates, in spite of their low C_{2+} selectivity. Moreover, the use of 2 wt% Mn/5 wt% Na_2WO_4 on SiO_2 as catalyst coated on top of the 3 BSCF_1010 layer rises X_{CH4} from 2 to 7%, while maintaining S_{C2+}. This important increase in conversion may arise from the high activity of Mn-Na_2WO_4 on SiO_2, in spite of the low C_{2+}

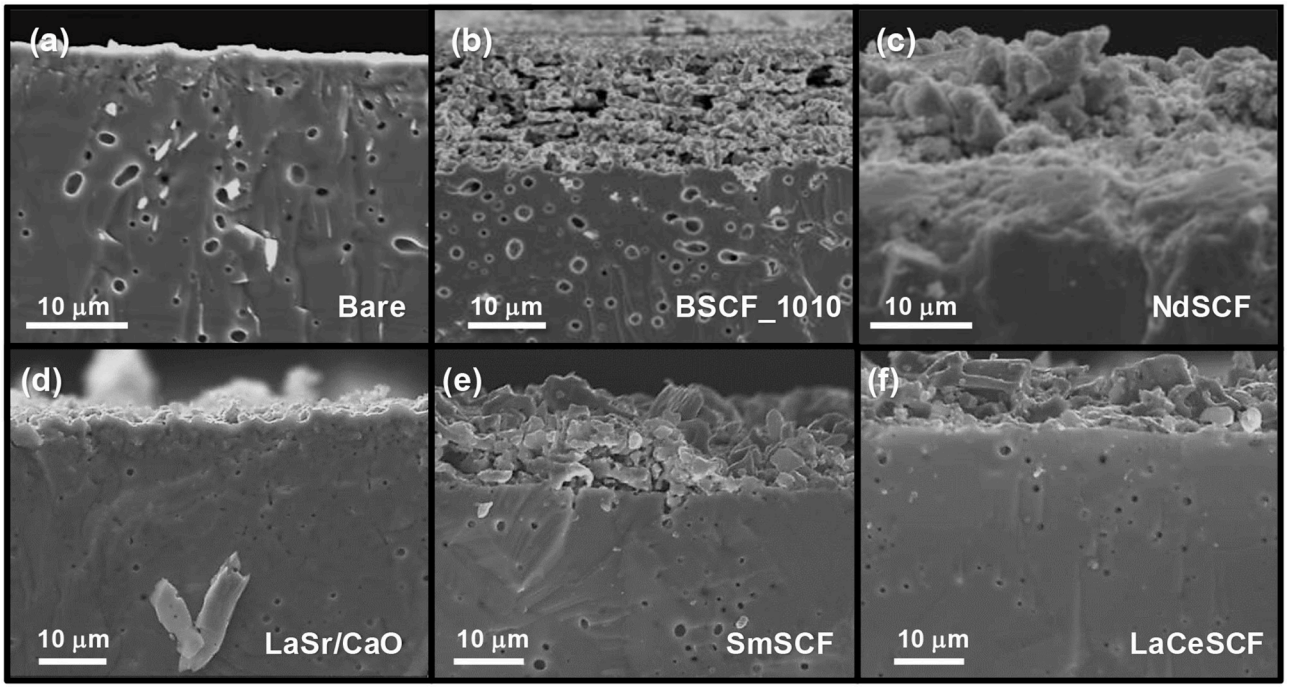

FIGURE 4 | SEM images of different BSCF-coated membranes: **(a)** bare, **(b)** BSCF initially sintered at 1,010°C, **(c)** NdSCF, **(d)** LaSr/CaO, **(e)** SmSCF, and **(f)** LaCeSCF.

production. Ceria based catalysts also present high conversion rates. Activation with CeTbO and CeGdO results in X_{CH4} of 5.3 and 6.5%, being higher than most of the tested perovskite catalysts. Again, the better redox properties and the higher ionic conductivity favor the conduction of OCM reaction.

The highest C_{2+} yields at 900°C (**Figure 5B**) range among 2.5–3% and correspond to CeTbO, CeGdO, LaCeSCF, and LaSr/CaO catalysts. On the other hand, maximum C_{2+} productivities correspond to LaCeSCF and CeTbO activated membranes. Their C_{2+} productivities of 0.37 $ml_{C2+}{\cdot}min^{-1}{\cdot}cm^{-2}$ represent nearly a four-fold improvement with respect to the non-activated membrane.

Further OCM tests were performed at 1,000°C maintaining the same feed and reactant gas flow rates as in the previous tests conducted at 900°C. Nevertheless, and due to the increase in temperature, the O_2 permeation of the membranes also increased (up to 2.2–2.6 $ml{\cdot}min^{-1}{\cdot}cm^{-2}$). This led to lower CH_4/O_2 ratios in the range of 4.8–5.6, and subsequently, to a significant increase in CH_4 conversion for all the catalysts, with a maximum X_{CH4} of 18.5% for the 3 BSCF_1010 Mn-Na_2WO_4 activated membrane (**Figure 6A**). The increase in temperature and the subsequent reduction in CH_4/O_2 ratios also allowed an improvement in C_{2+} selectivity (74%) for most of the catalysts, presenting values above 50%. This gain in X_{CH4} and S_{C2+} can also be ascribed to the higher generation of $CH_3^{\cdot}$ when operating at higher temperatures (Xu and Thomson, 1997). Again, the highest C_{2+} selectivity is reached with BSF_1010 catalytic layer. As can be seen in **Figure 6B**, operation at 1,000°C produces an important shift in C_{2+} yield and productivity, with a peak yield of nearly 9% when considering CeTbO activation. C_{2+} yields >8.7% are also obtained with CeGdO and 3 BSCF_1010 Mn-Na_2WO_4 catalysts. A maximum of C_{2+} productivity of 1.14 $ml_{C2+}{\cdot}min^{-1}{\cdot}cm^{-2}$ is obtained with CeTbO. According to the 30% yield target established for considering OCM reaction as techno-economically viable, the obtained results are far below this threshold, despite the good C_{2+} selectivities obtained for some of the catalysts.

In a previous study, Zeng and Lin observed a relation between CMR configuration and OCM reaction performance, reporting an improvement in C_{2+} yield from 11 to 17% by increasing membrane surface area to reactor volume ratio (Zeng and Lin, 2001). Indeed, issues such as reactor design/configuration and inadequate reactant gas distribution can prevent the proper access of CH_4 molecules to the active sites, thus limiting methane conversion rates. Therefore, OCM studies on BSCF tubular membranes reactor were also considered. Tubular designs provide a distributed feed of O_2 along the reactor length and a higher surface reaction area, leading to higher CH_4 conversion rates per membrane unit length, and increasing C_{2+} yields. A catalytic packed-bed consisting of 50% vol. 2% Mn, 5% Na_2WO_4 on SiO_2 and SiC was prepared for the activation of a BSCF capillary. OCM tests were carried out at 900°C, 200 $ml{\cdot}min^{-1}$ of synthetic air feed, and using a stream of 10% CH_4 in argon as reactant gas. The reactant gas flow rates varied from 50 to 600 $ml{\cdot}min^{-1}$, corresponding to CH_4/O_2 ratios of 1 and 2.7, respectively. As a result, X_{CH4}

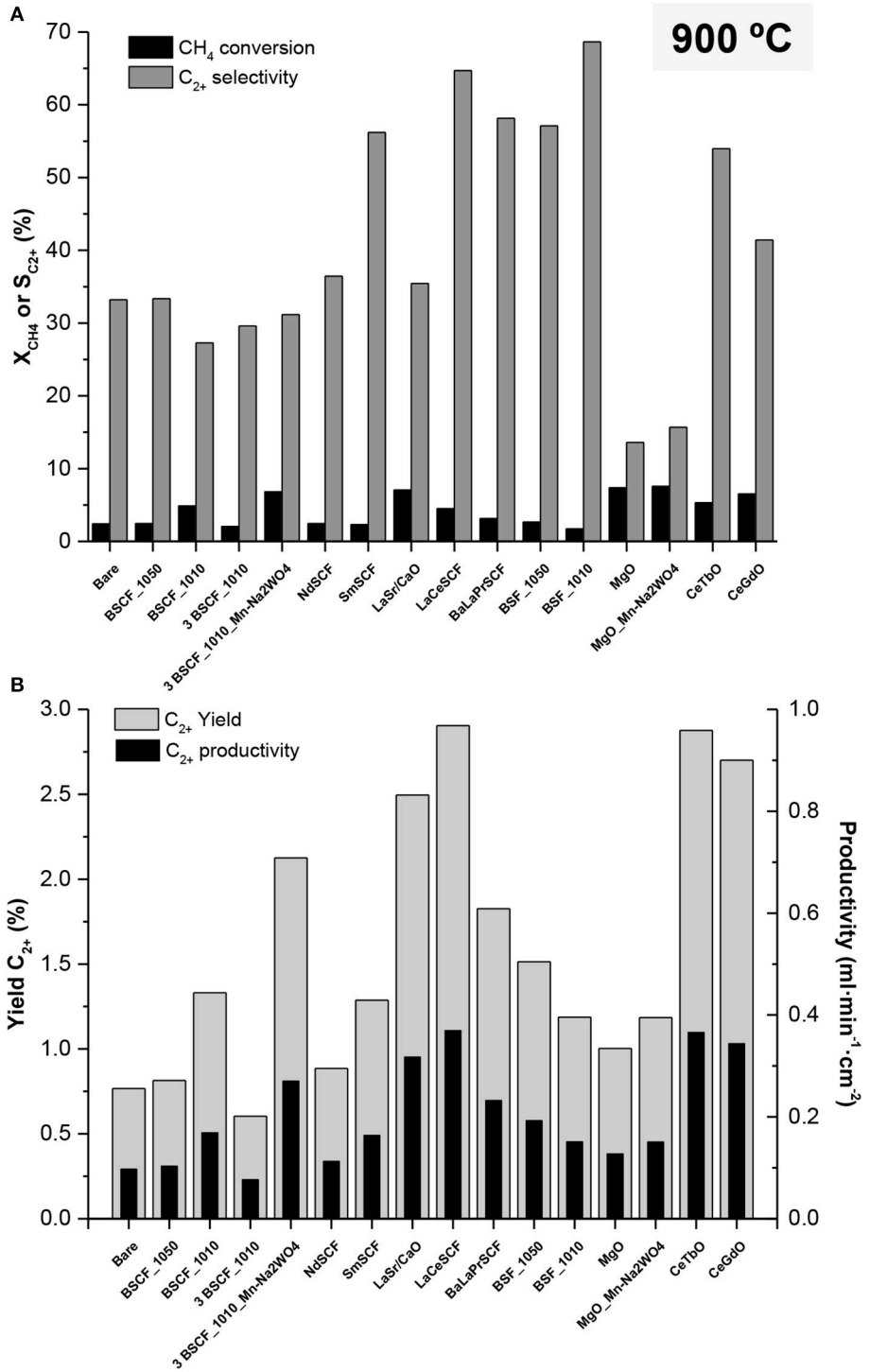

FIGURE 5 | (A) CH_4 conversion and selectivity to C_{2+}-hydrocarbon and **(B)** yield to C_{2+}-hydrocarbon for different planar BSCF membrane reactors at 900°C. 10% of CH_4, $Q_{(CH4+Ar)} = 100$ ml·min^{-1}, $Q_{Air} = 200$ ml·min^{-1} ($pO_2 = 0.21$ bar).

progressively decreased (**Figure 7**) when increasing reactant flow rate, thus evidencing the effect of the higher CH_4/O_2 ratio. Nevertheless, the lower residence time resulting from the increase in reactant gas flow rate is also expected to affect negatively CH_4 reaction. Differently, C_{2+} selectivity progressively improves with increasing reactant gas flow rate, with a maximum of ca.

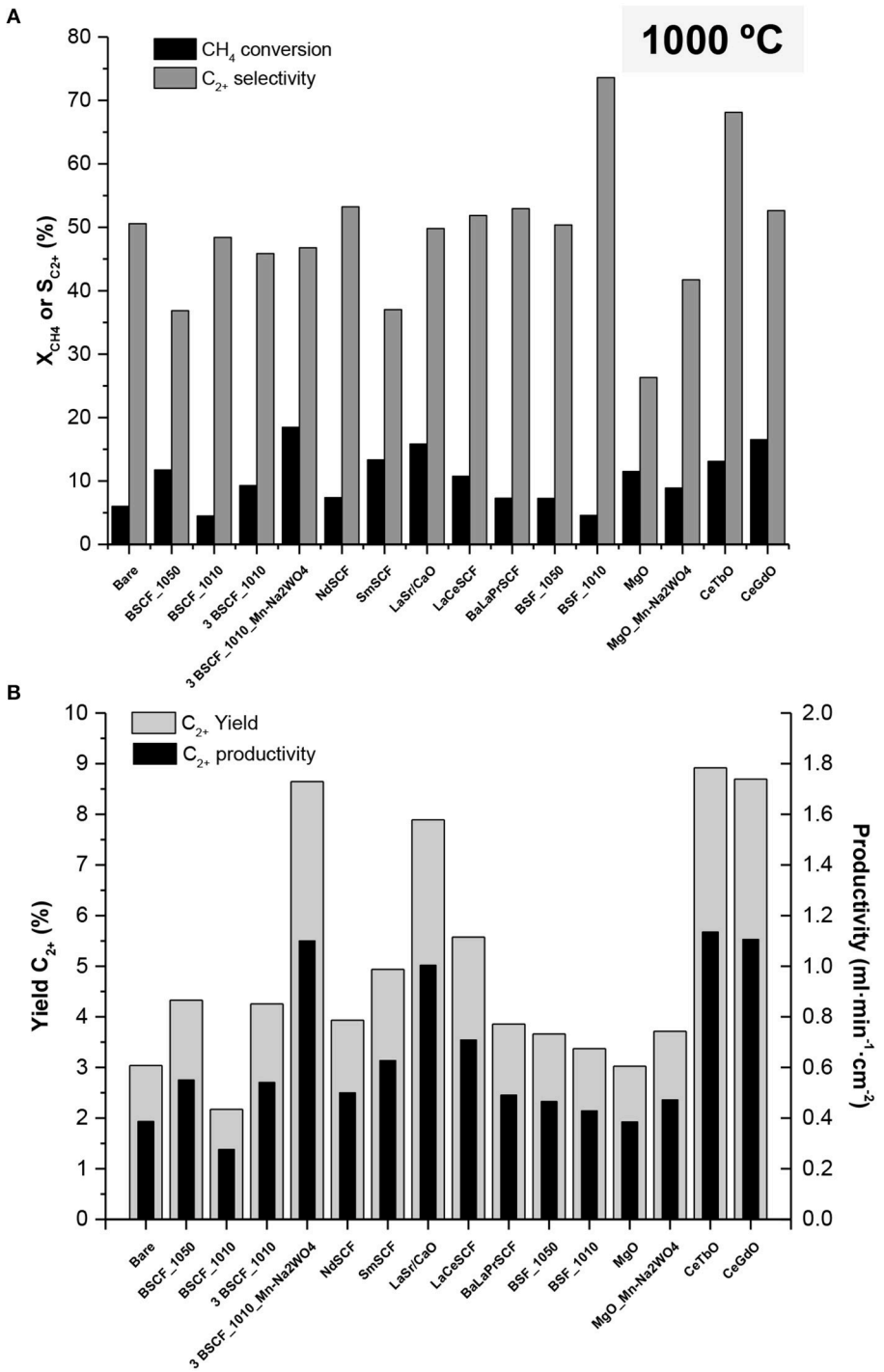

FIGURE 6 | (A) CH_4 conversion and selectivity to C_{2+}-hydrocarbon and **(B)** yield to C_{2+}-hydrocarbon for different planar BSCF membrane reactors at 1,000°C. 10% of CH_4, $Q_{(CH4+Ar)} = 100$ ml·min^{-1}, $Q_{Air} = 200$ ml·min^{-1} ($pO_2 = 0.21$ bar).

45% at 600 ml·min^{-1}. The highest C_{2+} yield is achieved at 100 ml·min^{-1} with a value of 15.6% at a CH_4 conversion of 54% and a C_{2+} selectivity of 29%. Concerning C_{2+} productivity, 0.9 ml·min^{1}·cm^{-2} are obtained with a flow rate of 400 ml·min^{-1}. On the other hand, low space velocities involve higher S_{CO2}, due to a higher CH_4 oxidation toward CO_2 at higher residence times. As the main interest of this reaction is the production of C_{2+}, then the most suitable conditions would be set at

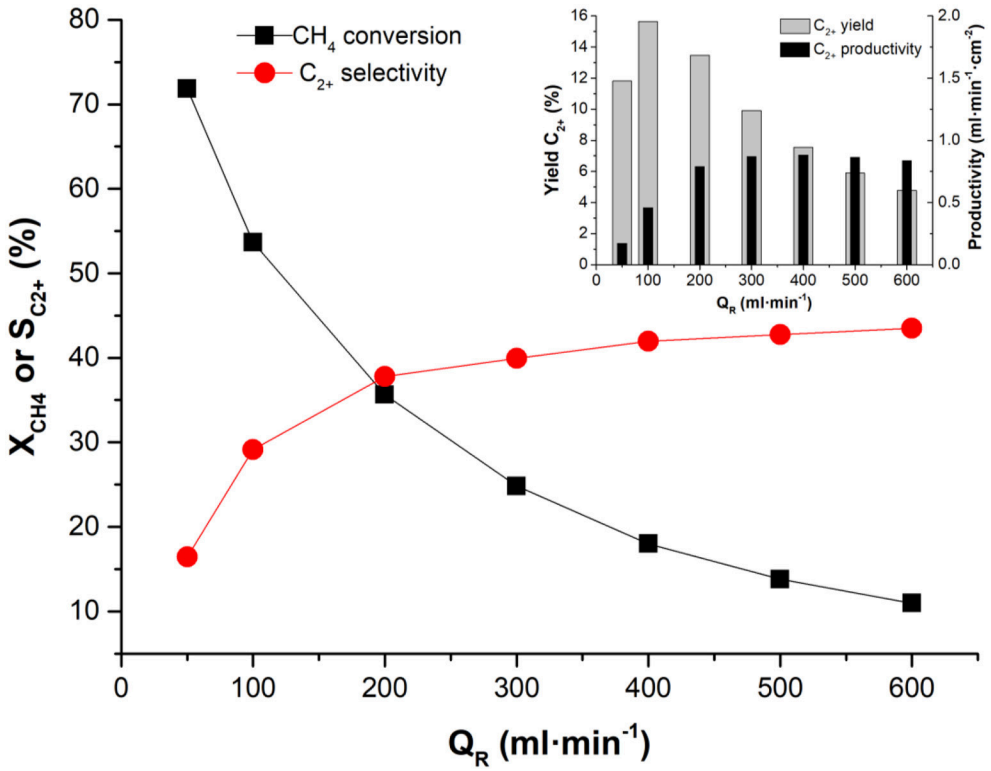

FIGURE 7 | Effect of the variation of reactant gas flow rate on X_{CH4} and S_{C2+}, and on Y_{C2+} and $C_{2+}H_4$ productivity (Inset). Test conducted at 900°C with 200 ml·min^{-1} synthetic air feeding and 10% CH_4 in Ar.

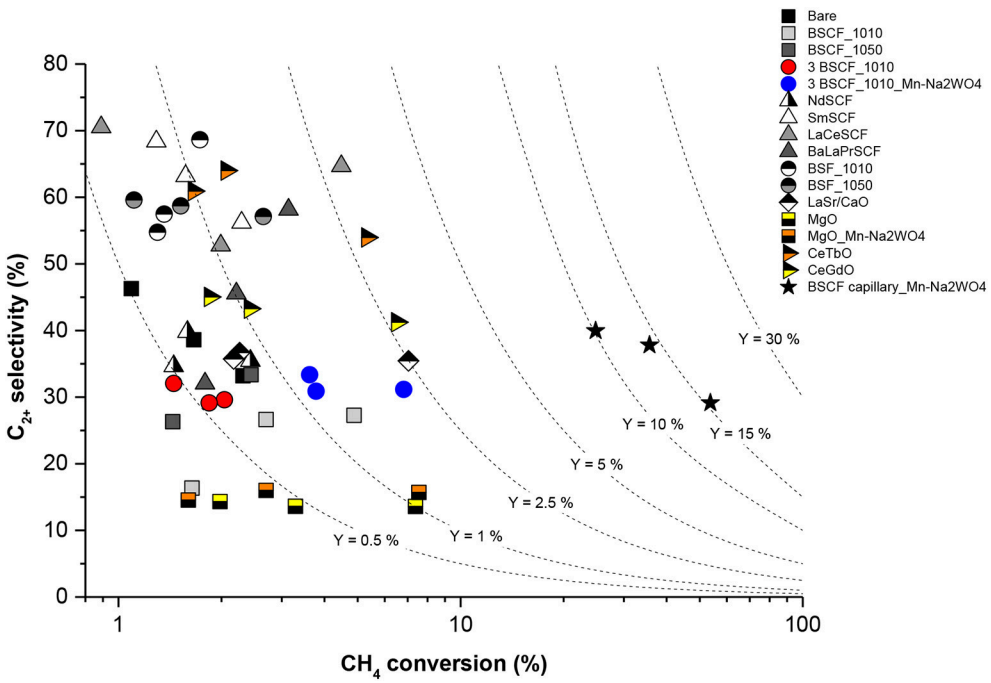

FIGURE 8 | C_{2+} hydrocarbon selectivity in dependence of methane conversion for different activated BSCF membranes. Test conditions: 900°C, synthetic air feeding (200 ml·min^{-1}), 10% CH_4 in argon as reactant gas (100–300 ml·min^{-1}).

low space velocities, with flow rates in the range of 50–200 $ml \cdot min^{-1}$.

Finally, **Figure 8** summarizes and compares the results obtained for both planar and tubular BSCF CMRs considered in the present work, represented by the S_{C2+} as a function of the converted CH_4. These results were obtained at 900°C and reactant gas flow rates in the range of 100–300 $ml \cdot min^{-1}$. Under such conditions, planar membranes show CH_4/O_2 ratios in the range of 7.5–11, whereas tubular configuration presents much lower ratios of 1.7–2.4. Indeed, significant shift in X_{CH4} is visible when comparing planar and tubular CMRs activated with Mn-Na_2WO_4/SiO_2 catalyst due to the higher availability of O_2. While S_{C2+} of 30–40% was obtained for both cases, CH_4 conversion increased from 4 to 7% up to 60% when conducting OCM in the tubular reactor. This is due to the higher membrane surface area to reactor volume ratio of tubular configurations that allows the dosing of higher amounts of O_2. This eventually improves OCM performance by boosting CH_4 conversion, achieving C_{2+} yields of 15.6%. The best results regarding selectivity toward C_{2+} production correspond to planar membranes activated with BSF, LaCeSCF, and SmSCF, presenting selectivity of ca. 65–70%. Nevertheless, the low X_{CH4} rates lead to poor C_{2+} yields -ranging from 0.5 to 2.5%, which are very low for practical consideration. The better performance observed with the tubular CMR is mainly ascribed to the lower CH_4/O_2 ratios used during the tests, which results from the increase of membrane surface area with respect to reactor volume. Therefore, for a given reactor geometry, the increase of this parameter and the selection of operation conditions resulting in higher CH_4/O_2 ratios can lead to the achievement of higher C_{2+} yields. For our reactor, the high conversions of nearly 60% obtained with the tubular CMR combined with the high C_{2+} selectivity of catalysts like LaCeSCF or SmSCF set a promising scenario for reaching the considered C_{2+} yield target of 30% if these catalysts are used for the activation of BSCF capillary membranes.

CONCLUSIONS

A study on oxidative coupling of methane for the production of ethylene was conducted considering CMR based on BSCF. In a first approach, a catalytic screening in CMR for OCM was conducted on disk-shaped planar BSCF membranes. The catalytic activation of membranes with 15 different catalysts allowed the identification of the most active compounds on these temperature conditions for the maximization of C_{2+} production. The highest C_{2+} selectivity at 900°C was 70%, reached with BSF and LaCeSCF catalysts. Despite the good selectivity, the low CH_4 conversions resulted in C_{2+} yields below 3% for this CMR configuration. Operation at higher temperatures (e.g., 1,000°C) produced a significant improvement in X_{CH4} for all the activated membranes due to the decrease in CH_4/O_2 ratios, thus obtaining much higher C_{2+} yields of up to nearly 9% and productivities of ca. 1.2 $ml \cdot min^{-1} \cdot cm^{-2}$ with CeGdO and 3 BSCF_1010 Mn-Na_2WO_4 catalysts. Conduction of OCM reaction on a catalytic membrane reactor with tubular geometry permitted the achievement of CH_4/O_2 ratios of 1.7–2.5 that improved C_{2+} yield, with a maximum of 15.6% at 900°C for a BSCF capillary activated with 2 wt% Mn/5 wt% Na_2WO_4 on SiO_2 catalyst. This improvement is ascribed to the combined effect of the catalyst high activity toward CH_4 conversion and the higher membrane surface area available for the conduction of OCM reaction and favorable geometry, resulting in lower CH_4/O_2. Therefore, the selection of the most active catalysts under CMR conditions, the operation with low CH_4/O_2 ratios, and the addressing of actions for the improvement of CMR design would allow achieving higher C_{2+}, approaching techno-economic targets.

AUTHOR CONTRIBUTIONS

JS: project manager; JS, ML, MB, and JG-F: manuscript writing and results interpretation; ML, MB, and JG-F: experiments.

ACKNOWLEDGMENTS

Financial support by the Spanish Government (ENE2014-57651 and SEV-2012-0267 grants) and by the EU through FP7 GREEN-CC Project (GA 608524), is gratefully acknowledged. The authors want also acknowledge the Electron Microscopy Service from the Universitat Politècnica de València for their support in the SEM analysis performed in this work.

REFERENCES

Akin, F. T., and Lin, Y. S. (2002). Oxidative coupling of methane in dense ceramic membrane reactor with high yields. *AIChE J.* 48, 2298–2306. doi: 10.1002/aic.690481019

Amenomiya, Y., Birss, V. I., Goledzinowski, M., Galuszka, J., and Sanger, A. R. (1990). Conversion of methane by oxidative coupling. *Catal. Rev. Sci. Eng.* 32, 163–227. doi: 10.1080/01614949009351351

Asadi, A. A., Behrouzifar, A., Iravaninia, M., Mohammadi, T., and Pak, A. (2012). Preparation and oxygen permeation of $La_{0.6}Sr_{0.4}Co_{0.2}Fe_{0.8}O_{3-d}$ (LSCF) perovskite-type membranes: experimental study and mathematical modeling. *Indus. Eng. Chem. Res.* 51, 3069–3080. doi: 10.1021/ie202434k

Aseem, A., and Harold, M. P. (2018). C-2 yield enhancement during oxidative coupling of methane in a nonpermselective porous membrane reactor. *Chem. Eng. Sci.* 175, 199–207. doi: 10.1016/j.ces.2017.09.035

Balaguer, M., Solis, C., and Serra, J. M. (2011). Study of the transport properties of the mixed ionic electronic conductor $Ce_{1-x}Tb_xO_{2-d}$ + Co (x = 0.1, 0.2) and evaluation as oxygen-transport membrane. *Chem. Mater.* 23, 2333–2343. doi: 10.1021/cm103581w

Bhasin, M. M., McCain, J. H., Vora, B. V., Imai, T., and Pujadó, P. R. (2001). Dehydrogenation and oxydehydrogenation of paraffins to olefins. *Appl. Catal. A Gen.* 221, 397–419. doi: 10.1016/S0926-860X(01)00816-X

Bhatia, S., Thien, C. Y., and Mohamed, A. R. (2009). Oxidative coupling of methane (OCM) in a catalytic membrane reactor and comparison of its performance with other catalytic reactors. *Chem. Eng. J.* 148, 525–532. doi: 10.1016/j.cej.2009.01.008

Chen, J. Q., Bozzano, A., Glover, B., Fuglerud, T., and Kvisle, S. (2005). Recent advancements in ethylene and propylene production using the UOP/Hydro MTO process. *Catal. Today* 106, 103–107. doi: 10.1016/j.cattod.2005.07.178

Czuprat, O., Schiestel, T., Voss, H., and Caro, J. (2010). Oxidative coupling of methane in a BCFZ perovskite hollow fiber membrane reactor. *Indus. Eng. Chem. Res.* 49, 10230–10236. doi: 10.1021/ie100282g

Erskine, K. M., Meier, A. M., and Pilgrim, S. M. (2002). Brazing perovskite ceramics with silver/copper oxide braze alloys. *J. Mater. Sci.* 37, 1705–1709. doi: 10.1023/A:1014912923977

Farrell, B. L., Igenegbai, V. O., and Linic, S. (2016). A viewpoint on direct methane conversion to ethane and ethylene using oxidative coupling on solid catalysts. *ACS Catal.* 6, 4340–4346. doi: 10.1021/acscatal.6b01087

Grubert, G., Kondratenko, E., Kolf, S., Baerns, M., van Geem, P., and Parton, R. (2003). Fundamental insights into the oxidative dehydrogenation of ethane to ethylene over catalytic materials discovered by an evolutionary approach. *Catal. Today* 81, 337–345. doi: 10.1016/S0920-5861(03)00132-9

Hutchings, G. J., Scurrell, M. S., and Woodhouse, J. R. (1989). Oxidative coupling of methane using oxide catalysts. *Chem. Soc. Rev.* 18, 251–283. doi: 10.1039/cs9891800251

Ito, T., and Lunsford, J. H. (1985). Synthesis of ethylene and ethane by partial oxidation of methane over lithium-doped magnesium-oxide. *Nature* 314, 721–722. doi: 10.1038/314721b0

Karakaya, C., Zhu, H., Zohour, B., Senkan, S., and Kee, R. J. (2017). Detailed reaction mechanisms for the oxidative coupling of methane over La_2O_3/CeO_2 nanofiber fabric catalysts. *Chemcatchem* 9, 4538–4551. doi: 10.1002/cctc.201701172

Keil, F. J. (1999). Methanol-to-hydrocarbons: process technology. *Micropor. Mesopor. Mater.* 29, 49–66. doi: 10.1016/S1387-1811(98)00320-5

Keller, G. E., and Bhasin, M. M. (1982). Synthesis of ethylene via oxidative coupling of methane: I. Determination of active catalysts. *J. Catal.* 73, 9–19. doi: 10.1016/0021-9517(82)90075-6

Lobera, M. P., Balaguer, M., Garcia-Fayos, J., and Serra, J. M. (2012a). Rare earth-doped ceria catalysts for ODHE reaction in a catalytic modified MIEC membrane reactor. *Chemcatchem* 4, 2102–2111. doi: 10.1002/cctc.201200212

Lobera, M. P., Balaguer, M., García-Fayos, J., and Serra, J. M. (2017). Catalytic oxide-ion conducting materials for surface activation of $Ba_{0.5}Sr_{0.5}Co_{0.8}Fe_{0.2}O_{3-\delta}$ membranes. *ChemistrySelect* 2, 2949–2955. doi: 10.1002/slct.201700530

Lobera, M. P., Escolástico, S., Garcia-Fayos, J., and Serra, J. M. (2012b). Ethylene production by ODHE in catalytically modified $Ba_{0.5}Sr_{0.5}Co_{0.8}Fe_{0.2}O_{3-d}$ membrane reactors. *Chemsuschem* 5, 1587–1596. doi: 10.1002/cssc.201100747

Lobera, M. P., Escolastico, S., and Serra, J. M. (2011). High ethylene production through oxidative dehydrogenation of ethane membrane reactors based on fast oxygen-ion conductors. *Chemcatchem* 3, 1503–1508. doi: 10.1002/cctc.201100055

Lunsford, J. H. (1995). The catalytic oxidative coupling of methane. *Angew. Chem. Int. Edn. Engl.* 34, 970–980. doi: 10.1002/anie.199509701

Lunsford, J. H. (2000). Catalytic conversion of methane to more useful chemicals and fuels: a challenge for the 21st century. *Catal. Today* 63, 165–174. doi: 10.1016/S0920-5861(00)00456-9

Maitra, A. M. (1993). Critical performance evaluation of catalysts and mechanistic implications for oxidative coupling of methane. *Appl. Catal. Gen.* 104, 11–59.

Mleczko, L., and Baerns, M. (1995). Catalytic oxidative coupling of methane - reaction-engineering aspects and process schemes. *Fuel Process. Technol.* 42, 217–248. doi: 10.1016/0378-3820(94)00121-9

Mleczko, L., Pannek, U., Niemi, V. M., and Hiltunen, J. (1996). Oxidative coupling of methane in a fluidized-bed reactor over a highly active and selective catalyst. *Indus. Eng. Chem. Res.* 35, 54–61. doi: 10.1021/ie950145s

Olivier, L., Haag, S., Mirodatos, C., and van Veen, A. C. (2009). Oxidative coupling of methane using catalyst modified dense perovskite membrane reactors. *Catal. Today* 142, 34–41. doi: 10.1016/j.cattod.2009.01.009

Othman, N. H., Wu, Z., and Li, K. (2015). An oxygen permeable membrane microreactor with an in-situ deposited $Bi_{1.5}Y_{0.3}Sm_{0.2}O_{3-\delta}$ catalyst for oxidative coupling of methane. *J. Membr. Sci.* 488, 182–193. doi: 10.1016/j.memsci.2015.04.027

Otsuka, K., Jinno, K., and Morikawa, A. (1986). Active and selective catalysts for the synthesis of C_2H_4 and C_2H_6 via oxidative coupling of methane. *J. Catal.* 100, 353–359. doi: 10.1016/0021-9517(86)90102-8

Pak, S., Qiu, P., and Lunsford, J. H. (1998). Elementary reactions in the oxidative coupling of methane over $Mn/Na_2WO_4/SiO_2$and $Mn/Na_2WO_4/MgO$ catalysts. *J. Catal.* 179, 222–230. doi: 10.1006/jcat.1998.2228

Palermo, A., Holgado Vazquez, J. P., Lee, A. F., Tikhov, M. S., and Lambert, R. M. (1998). Critical influence of the amorphous silica-to-cristobalite phase transition on the performance of $Mn/Na_2WO_4/SiO_2$ catalysts for the oxidative coupling of methane. *J. Catal.* 177, 259–266. doi: 10.1006/jcat.1998.2109

Reporters, P. (2016). *The Ethylene Technology Report 2016*. Available online at: www.researchandmarkets.com

Schulz, M., Pippardt, U., Kiesel, L., Ritter, K., and Kriegel, R. (2012). Oxygen permeation of various archetypes of oxygen membranes based on BSCF. *AIChE J.* 58, 3195–3202. doi: 10.1002/aic.13843

Spallina, V., Velarde, I. C. J., Jimenez, A. M., Godini, H. R., Gallucci, F. M., and Annaland, V. S. (2017). Techno-economic assessment of different routes for olefins production through the oxidative coupling of methane (OCM): advances in benchmark technologies. *Energy Convers. Manage.* 154, 244–261. doi: 10.1016/j.enconman.2017.10.061

Stansch, Z., Mleczko, L., and Baerns, M. (1997). Comprehensive kinetics of oxidative coupling of methane over the La_2O_3/CaO catalyst. *Indus. Eng. Chem. Res.* 36, 2568–2579. doi: 10.1021/ie960562k

Sunarso, J., Baumann, S., Serra, J. M., Meulenberg, W. A., Liu, S., Lin, Y. S., et al. (2008). Mixed ionic-electronic conducting (MIEC) ceramic-based membranes for oxygen separation. *J. Membr. Sci.* 320, 13–41. doi: 10.1016/j.memsci.2008.03.074

Tan, X., and Li, K. (2006). Oxidative coupling of methane in a perovskite hollow-fiber membrane reactor. *Indus. Eng. Chem. Res.* 45, 142–149. doi: 10.1021/ie0506320

Tan, X., Pang, Z., Gu, Z., and Liu, S. (2007). Catalytic perovskite hollow fibre membrane reactors for methane oxidative coupling. *J. Membr. Sci.* 302, 109–114. doi: 10.1016/j.memsci.2007.06.033

Tenelshof, J. E. H., Bouwmeester, J. M., and Verweij, H. (1995). Oxidative coupling of methane in a mixed-conducting perovskite membrane reactor. *Appl. Catal. Gen.* 130, 195–212.

Thaler, F., Müller, M., and Spatschek, R. (2016). Oxygen permeation through perovskitic membranes: the influence of steam in the sweep on the permeation performance. *AIMS Mater. Sci.* 3, 1126–1137. doi: 10.3934/matersci.2016.3.1126

Wang, D. J., Rosynek, M. P., and Lunsford, J. H. (1995). Oxidative coupling of methane over oxide-supported sodium-manganese catalysts. *J. Catal.* 155, 390–402. doi: 10.1006/jcat.1995.1221

Wang, H., Cong, Y., and Yang, W. (2005). Oxidative coupling of methane in $Ba_{0.5}Sr_{0.5}Co_{0.8}Fe_{0.2}O_{3-\delta}$ tubular membrane reactors. *Catal. Today* 104, 160–167. doi: 10.1016/j.cattod.2005.03.079

Xu, S. J., and Thomson, W. J. (1997). Perovskite-type oxide membranes for the oxidative coupling of methane. *AIChE J.* 43, 2731–2740. doi: 10.1002/aic.690431319

Zeng, Y., and Lin, Y. S. (2001). Oxidative coupling of methane on improved bismuth oxide membrane reactors. *AIChE J.* 47, 436–444. doi: 10.1002/aic.690470220

Zeng, Y., Lin, Y. S., and Swartz, S. L. (1998). Perovskite-type ceramic membrane: synthesis, oxygen permeation and membrane reactor performance for oxidative coupling of methane. *J. Membr. Sci.* 150, 87–98. doi: 10.1016/S0376-7388(98)00182-3

Zhou, W., Ran, R., Shao, Z., Zhuang, W., Jia, J., Gu, H., et al. (2008). Barium- and strontium-enriched $(Ba_{0.5}Sr_{0.5})_{1+x}Co_{0.8}Fe_{0.2}O_{3-\delta}$ oxides as high-performance cathodes for intermediate-temperature solid-oxide fuel cells. *Acta Mater.* 56, 2687–2698. doi: 10.1016/j.actamat.2008.02.002

Conflict of Interest Statement: The authors declare that the research was conducted in the absence of any commercial or financial relationships that could be construed as a potential conflict of interest.